0026-895X/93/010180-11$03.00/0

MOLECULAR PHARMACOLOGY, 44:180-190

Barium Blockade of a Clonal Potassium Channel and Its Regulation by a Critical Pore Residue

MAURIZIO TAGLIALATELA, JOHN A. DREWE, and ARTHUR M. BROWN

Department of Molecular Physiology and Biophysics, Baylor College of Medicine, Houston, Texas 77030

Received January 6, 1993; Accepted April 8, 1993

SUMMARY

Barium ion (Ba^{2+}) has the same crystal radius as potassium ion but blocks rather than permeates the ion-conducting pore of K^+ channels. Ba^{2+} ion may therefore be used as a probe of residues lining the pore of K^+ channels, and we applied it to test the position and function of a residue crucial for K^+/Rb^+ selectivity and blockade by internal tetraethylammonium. We examined blockade by internal and external Ba^{2+} of the delayed rectifier K^+ channel DRK1 (Kv2.1) and tested the effects of point mutations at pore residue 374. Internal Ba^{2+} blocked the wild-type open channel with high affinity (K_d = 13 μM). Blockade involved more than one site, was voltage dependent, and increased at more positive potentials. Mutation of V374 to threonine or serine produced a significant decrease in the rate of dissociation of internal Ba^{2+} from the pore, whereas mutation of V374 to isoleucine produced no change. For wild-type channels, external Ba^{2+} decreased the rate of activation of the K^+ current, suggesting that Ba^{2+} can interact with closed DRK1 channels. This result was unaffected by the V374T substitution. Furthermore, external Ba^{2+} also caused a very low affinity ($K_d \approx 30$ mM) and voltage-independent block of the open DRK1 channel. Thus, Ba^{2+} blocked the pore at internal and external sites, which were clearly distinguishable. The effects of substitution at position 374 with residues having polar hydroxyls are consistent with position 374 being at a surface position critical for ion permeation, near the inner mouth of the pore.

Pharmacological agents have long been useful experimental probes of voltage-dependent ion channels and in recent years their value has been enhanced by their application to cloned channels. For voltage-dependent K^+ channels, studies using charybdotoxin (1) and TEA (2–4) have been particularly useful, especially when combined with mutational analyses. These and other studies have identified residues primarily involved in ion conduction (3, 5–7), leading to the hypothesis that a highly conserved region between the putative transmembrane segments 5 and 6, called the S_5-S_6 linker or SS_1-SS_2 region (8, 9), forms the pore. However, charybdotoxin and TEA are large blocking molecules and do not probe deeper pore structures through which the K^+ ion must pass. A more suitable molecule for these purposes is Ba^{2+} ion, which has the same crystal radius as K^+ ion but is essentially impermeant in K^+ channels (10–15).

In the present investigation, we probed the structure of the cloned delayed rectifier DRK1 or Kv2.1 (16) with Ba^{2+} and used single-channel measurements along with point mutations to identify ion binding sites in the pore. We identified an external site at which a relatively fast, low affinity, voltage-independent blockade occurred and internal sites at which a cooperative, slower, high affinity, voltage-dependent blockade occurred. A multisite blocking model reproduced the main features of internal blockade. Internal but not external blockade was enhanced by substituting the polar residues serine and threonine for valine at position 374 in the primary sequence of the channel. The residue at this position is an important determinant of the pore phenotype and appears to occupy a surface position in K^+ pores.

This work was supported by National Institutes of Health Grants NS23877 and HL36930 to A.M.B.

Materials and Methods

Standard Recombinant DNA Techniques and Site-Directed Mutagenesis

The mutant versions of DRK1 (16), i.e., V374T, V374S, and V374I, were generated by site-directed mutagenesis, using an Amersham kit, as already described (17). Briefly, to obtain a single-stranded DNA template for specific oligonucleotide-directed mutagenesis, DRK1 was first digested with *Bam*HI (at positions +909 and +1520). The resulting 611-nucleotide fragment was subcloned into *Bam*HI-digested M13 mp19 single-stranded phagemid. Complementary oligonucleotides of 20–30 bases in length were synthesized (Applied Biosystem) with a 1–3-base mismatch for each of the mutant constructs. The mutated DNA fragment was cloned back into the original *Bam*HI-cut DRK1. The region spanning the *Bam*HI sites was then sequenced, to verify the presence of the mutation (18).

ABBREVIATIONS: TEA, tetraethylammonium; MES, 2-(*N*-morpholino)ethanesulfonic acid; HEPES, 4-(2-hydroxyethyl)-1-piperazineethanesulfonic acid; EGTA, ethylene glycol bis(β-aminoethyl ether)-*N*,*N*,*N*′,*N*′-tetraacetic acid.

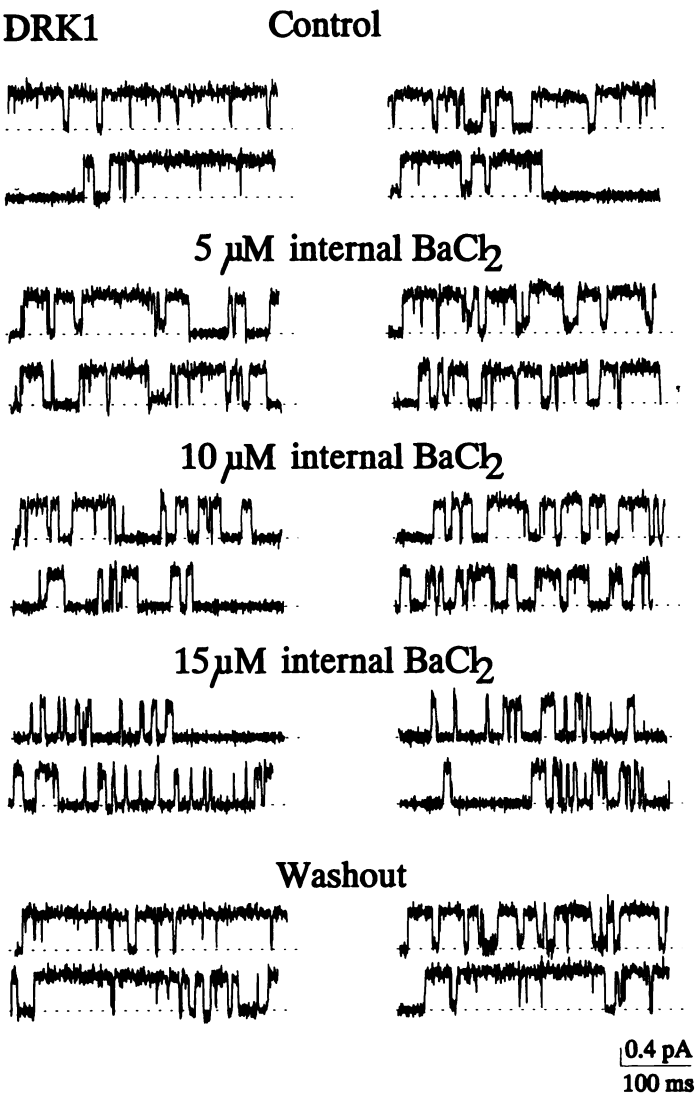

Fig. 1. Effect of internal Ba^{2+} on DRK1 single-channel currents. Representative single-channel *traces* obtained from the same DRK1-containing inside-out patch exposed to the indicated concentrations of internal free Ba^{2+} ions (from *top* to *bottom*, 0, 5, 10, 15, and 0 μM). Holding potential, −80 mV; test potential, +40 mV; sampling, 5 kHz; filter, 1 kHz.

In Vitro Transcription of the mRNAs and Oocyte Injection

Preparation of cRNAs using the T7 RNA polymerase and *in vitro* capping of the RNAs has been described previously (19). Stage V-VI *Xenopus* oocytes were injected with 75 nl of 10–100 ng/μl cRNA in 0.1 M KCl and were incubated at 19° in modified Barth's solution. For whole-cell measurements, the follicular layer surrounding the eggs was manually removed at least 4 hr before recording. For single-channel recording, the vitelline membrane also was manually removed.

Electrophysiology

Single-channel currents. Single-channel currents were recorded from cell-attached and inside-out membrane patches using oocytes dissected free of the vitelline envelope and micropipettes of 2–5-MΩ resistance that had been fire-polished and coated with Sylgard (Dow-Corning, Midland, MI). The pipette solution contained (in mM) 120 NaCl, 2.5 KCl, 2 $MgCl_2$, and 10 HEPES, pH 7.2. Holding and test potentials applied to the membrane patch are reported as conventional absolute intracellular potentials, assuming that the oocyte resting potential was zeroed by the bathing solution, which contained (in mM) 100 KCl, 10 EGTA, and 10 HEPES, pH 7.2. Data were low-pass filtered at 0.5–1 kHz (−3 dB, four-pole Bessel filter) before digitization at 2 or 5 kHz. Channels were activated with rectangular test pulses from negative holding potentials. Holding potentials were adjusted to minimize simultaneous overlapping openings in patches containing more than one channel. Current records were corrected for capacitative and leakage currents by subtracting the smoothed average of records lacking channel activity. The appropriate desired concentrations of Ba^{2+} were obtained by diluting concentrated stock solutions of $BaCl_2$ (from 0.01 to 1 M) directly either in the pipette-filling solution (exposed to the external side of the membrane in the cell-attached configuration) or in the bath solution (exposed to the internal side of the membrane in the inside-out configuration). Throughout the manuscript, the values of free Ba^{2+} concentrations are reported, calculated in the case of internal Ba^{2+} from the total Ba^{2+} concentrations and the dissociation constant for the EGTA-Ba^{2+} complex (20).

Data were analyzed as follows. Single-channel currents were idealized by using an algorithm that uses a dI/dt threshold for identifying transitions between closed and open states (21). In a second pass through the idealized data, idealized openings were constructed using a threshold set at one half the amplitude of the unitary current. Open and closed interval durations of the idealized data were collected into distribution histograms. These histograms were fit by sums of exponentials using a maximum likelihood estimate. Events of <0.5-msec duration were excluded from the histogram to avoid truncation errors introduced by the limited frequency response of the system. Waiting time distributions were obtained from the latency between the beginning of the test pulse and the first channel opening detected in the record and were fit by a sum of exponentials using a maximum likelihood estimate. Where appropriate, data are expressed as mean ± standard error. Both whole-cell and single-channel experiments were performed at room temperature (22–24°) in a recording chamber that was continuously superfused with bath solution at a rate of 2 ml/min.

Whole-cell measurements. Two to 5 days after the injection, the follicular cell layer was manually removed and oocytes were voltage-clamped using a commercial two-electrode voltage-clamp amplifier (Dagan 8500; Dagan Corp.). Both the current and voltage electrodes were filled with 3 M KCl, 10 mM HEPES, pH 7.4. To reduce outward Cl^- currents, the external solution contained 100 mM *N*-methyl-D-glucamine, 100 mM MES, 2.5 mM KOH, 2 mM $Mg(OH)_2$, and 10 mM HEPES, pH 7.4, except in the experiments of Fig. 9C (see the corresponding figure legend). The resistance of the current electrode was 1–2 MΩ and that of the voltage electrode varied between 2 and 5 MΩ. No compensation for the oocyte series resistance was performed. The PClamp system (Axon Instruments) was used for generation of the voltage pulse protocols and for data acquisition. Linear leakage and capacity currents were corrected on-line by using the $P/4$ subtraction method.

Model Simulation

Single-channel currents simulating the state diagram of the model shown in Fig. 11 were obtained using the CSIM software (Axon Instruments). The effect of increasing internal Ba^{2+} concentrations was simulated by varying simultaneously and proportionally the forward rates for Ba^{2+} association (k_{1Ba1}, k_{2Ba2}, and k_{3Ba3}).

The idealized events from 100 simulated single-channel traces for each Ba^{2+} concentration (0, 5, 10, 15, 20, and 25 μM) were collected into probability of being open versus time plots and open time histograms. The concentration dependence of the effects of Ba^{2+} on the channel probability of being open and open time (fit using a single-exponential function) is shown in Fig. 11, B and C.

Results

Internal Blockade of DRK1 Single-Channel Currents by Ba^{2+}

When the cytoplasmic face of inside-out membrane patches from oocytes expressing wild-type DRK1 channels was perfused with micromolar concentrations of Ba^{2+}, a dramatic alteration of single-channel currents was observed; the relatively long

openings observed under control conditions were shortened and interrupted by long-lived closing events (Fig. 1). The latency to first opening was not affected; at +40 mV it was 32.1 ± 3.9 msec (n = 6) in controls and 34.2 ± 7.4 msec (n = 6) with 15 μM Ba^{2+}. Single-channel current amplitude was unaffected except at concentrations greater than 15 μM and potentials greater than +40 mV. For example, at +60 mV the single-channel amplitude was decreased from 1.08 ± 0.03 pA (n = 4) to 0.91 ± 0.03 (n = 4) by 15 μM Ba^{2+}, whereas at 0 mV the mean current values were 0.43 ± 0.01 pA (n = 7) and 0.42 ± 0.01 pA (n = 6) in the absence and in the presence of 15 μM Ba^{2+}, respectively. The block was more pronounced at depolarized potentials, indicating that it was voltage dependent.

Concentration Dependence of the Internal Blockade by Ba^{2+}

The dose dependence of the internal blockade by Ba^{2+}, estimated from changes in the probability of being open as a function of Ba^{2+} concentration, is shown in Fig. 2A. The dose-response relationship was much steeper than expected for a model in which Ba^{2+} ion interacts with a single site. From the data shown in Fig. 2A, we calculated a dissociation constant, K_d, of 13 μM and a Hill coefficient of 3, indicating more than one internal site with cooperativity among the sites. However, the Hill coefficient may not equal the number of binding sites and is a more complex representation that includes the number of sites and interaction among sites (22). The complexity of this interaction is also suggested by the observation that the data seem to be consistent with a smaller (between 2 and 3) Hill coefficient at lower concentrations and with a larger one (between 3 and 4) at higher concentrations.

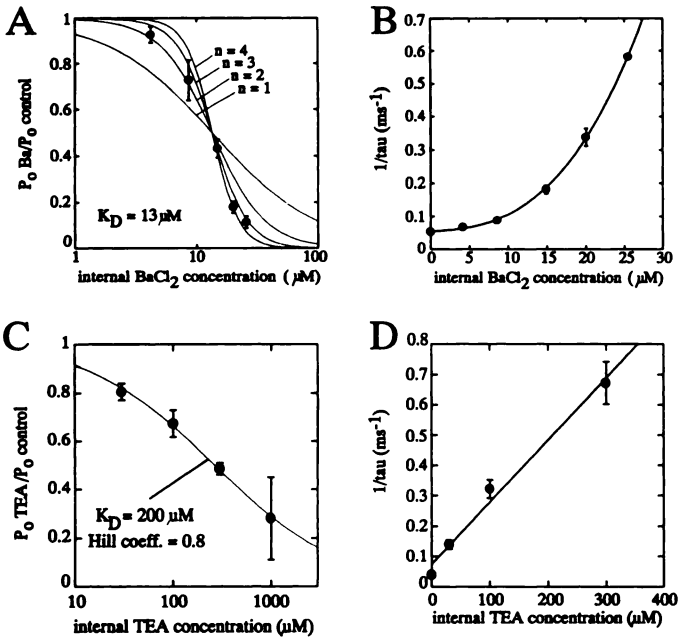

Fig. 2. Concentration dependence of internal Ba^{2+} and TEA block of DRK1 channels. A and C, Dose-response relationship for internal Ba^{2+}-induced (A) and TEA-induced (C) block of DRK1 single-channel currents. Single-channel currents at different internal Ba^{2+} and TEA concentrations were integrated, and the integrated value was expressed as a fraction of the control value. The *four solid lines* in A are fits of the *experimental points* to the equation $\max/(1 + (x/k)^n)$, where k is the K_d for the block (13 μM) and n is the Hill coefficient (assumed value of 1, 2, 3, or 4). Each *point* is the mean ± standard error of at least four determinations. B and D, Reciprocal of the mean open time plotted as a function of the internal Ba^{2+} (B) or TEA (D) concentration. Each *point* is the mean ± standard error of at least four determinations. In C, the *solid line* represents a polynomial equation fitted to the *experimental points*, to show the nonlinear concentration dependence of the on rate for Ba^{2+}. In D, the *solid line* represents a linear regression fitted to the *experimental points*, to show the linear concentration dependence of the on rate for TEA.

The kinetics of internal blockade were dose dependent and also were consistent with there being more than one site. If internal Ba^{2+} ions blocked in a simple bimolecular reaction following first-order kinetics, the reciprocal of the forward rate constant should be a linear function of the concentration of Ba^{2+} ion. From single-channel currents, we can estimate the association rate constant from the decrease of the channel mean open time. In Fig. 2B, we have plotted the reciprocal of the mean open time of DRK1 channels as a function of internal Ba^{2+} concentration. The results obtained clearly show that the relationship is nonlinear and that the kinetics of association of internally applied Ba^{2+} ions are more complex than would be predicted by a first-order bimolecular reaction. This suggests the presence of cooperativity among multiple sites, as predicted from the dose-response curve.

For comparison, the dose-response relationship for blockade by internal TEA is shown in Fig. 2C. Unlike internal Ba^{2+} ion, the Hill coefficient for internal TEA blockade was approximately 1, consistent with previous observations that a single TEA molecule can block cloned K^+ channels by binding to the external or the internal mouths of the pore (23–26). As anticipated for a single blocking site, there was a linear relationship between the reciprocal of the open times and the internal TEA concentration (Fig. 2D).

It was difficult to estimate the dissociation rate constant for Ba^{2+} ion, because the kinetics of blockade overlapped the gating kinetics. In the absence of Ba^{2+} ions, the closed times in DRK1 channels were described by a sum of three exponentials (Fig. 3A). At +40 mV, the mean values were 0.6 ± 0.17 msec (τ_1), 7.7 ± 0.8 msec (τ_2), and 48 ± 10 msec (τ_3) (mean ± standard error, n = 8 patches). The relative amplitudes were 57.9 ± 3.8%, 36.1 ± 3.4%, and 5.4 ± 0.8% for τ_1, τ_2, and τ_3, respectively (mean ± standard error, n = 8). With 15 μM internal Ba^{2+} (Fig. 3B), the closed time distribution was still fitted by a sum of three exponentials, with similar time constants (0.82 ± 0.4 msec, 12 ± 2.6 msec, and 61.6 ± 18 msec for τ_1, τ_2, and τ_3, respectively (mean ± standard error, n = 4). However, the relative proportion of the area under the exponentials was dramatically altered; the relative amplitudes were 26 ± 9.5%, 59.6 ± 16%, and 14.4 ± 8% for τ_1, τ_2, and τ_3, respectively (mean ± standard error, n = 4). We were therefore unable to identify a time constant in the closed time distribution that would correspond to the unblocking step, probably because this step was governed by a rate constant similar to that of channel gating. The increase in the amplitude of τ_2 depended upon both Ba^{2+} concentration and voltage, and these results led us to conclude that the closed times introduced by internal Ba^{2+} ions fell within the range of τ_2 (8–16 msec).

The concentration-dependent increase in the relative amplitude of τ_2 occurred mostly at the expense of the fastest time constant, τ_1. In contrast, the relative amplitude of τ_3 did not show significant decrease with increasing internal Ba^{2+} concentration (Fig. 3D). This result was clearly unexpected; once a new (blocked) state is introduced in the kinetic scheme, the occurrence of the other states should decrease. However, the limitations imposed by the low frequency of occurrence of

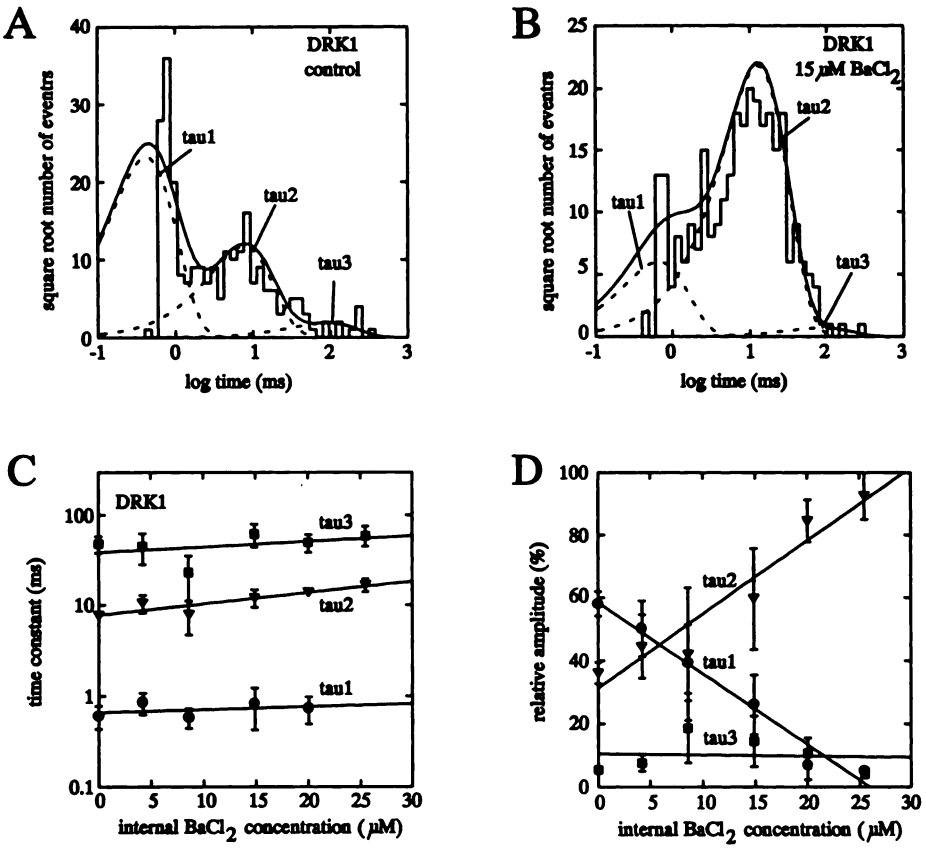

Fig. 3. Determination of the off rate for Ba^{2+} ions from single-channel closed time distributions. A and B, Distributions of the DRK1 single-channel closed intervals in the same inside-out patch under control conditions (A) or after exposure to 15 μM Ba^{2+} (B). In both cases, three exponentials were required to adequately fit the data. The three peaks were defined as τ_1, τ_2, and τ_3, which correspond to the fastest, middle, and slowest time constants of the distribution, respectively. Each *point* is the mean ± standard error of at least four determinations. C and D, Dependence on internal Ba^{2+} concentration of the three time constants of the closed time distribution (C) and of their relative amplitude (D). The *solid lines* represent linear regressions fitted to the *experimental points* for each of the exponentials (τ_1, τ_2, and τ_3). Each *point* is the mean ± standard error of at least four determinations.

events in the τ_3 range of the distribution caused uncertainty with respect to the effect of Ba^{2+} on its duration and relative amplitude. Unlike the concentration-dependent shortening of open time, the closed time τ values were only modestly affected by varying internal Ba^{2+} concentrations (Fig. 3C).

Voltage Dependence of Ba^{2+} Block of DRK1 Channels

In Fig. 4A are reported single-channel traces from DRK1 inside-out patches at two different voltages (+20 mV and +60 mV), both under control conditions and in the presence of 15 μM internal Ba^{2+}. The open time distributions for each of the four experimental conditions are shown in Fig. 4B. In all four cases the distributions were best fit with single-exponential functions. From the data shown, it seems clear that the mean channel open times in the presence of internal Ba^{2+} was decreased at higher voltages, whereas no voltage dependence was observed for the control channel mean open time between 0 and +60 mV.

In Fig. 5 the reciprocal of the mean open time, which measures the drug association (on) rate, is plotted as a function of membrane potential. The on rate for internal Ba^{2+} was increased with depolarization, whereas the on rate for external Ba^{2+} (see below) was not affected by changes in membrane potential. The on rate increased exponentially with depolarization (e-fold for 45 mV), consistent with an average electrical distance for the blocking site of about 30% of the distance from the cytoplasmic face of the channel.

The voltage dependence of the closed times in the absence and in the presence of Ba^{2+} is shown in Fig. 6. As already introduced, the closed time distribution in DRK1 channels was accurately described by a sum of three exponentials (τ_1, τ_2, and τ_3). Under control conditions no voltage dependence was found for any time constant (Fig. 6A). Furthermore, the relative amplitude of each of the three time constants did not vary significantly with changes in membrane potential (Fig. 6B). In contrast, in the presence of 15 μM Ba^{2+} ions the closed time histogram was still described by a sum of three exponentials (Fig. 6, C and D), but their relative amplitudes were dramatically altered by depolarization of the patch membrane. In fact, whereas depolarization decreased the relative amplitude of both the fastest (τ_1) and the slowest (τ_3) time constants, the proportional area of the middle time constant (τ_2) was increased by depolarization (Fig. 6D). These data confirm the idea that, at positive potentials and high Ba^{2+} concentrations, the reciprocal of τ_2 is a reliable measure of the reverse rate constant, which measures the speed of Ba^{2+} dissociation from the channel. A closer inspection of Fig. 6C reveals that τ_2 increased slightly with depolarization, suggesting that dissociation of internal Ba^{2+} was impeded at more positive potentials. We estimated an e-fold decrease in the off rate constant for 229 mV of membrane depolarization, which corresponds to an electrical distance of about 10% of the membrane field, from its inner margin (δ = 0.10). The existence of a small degree of voltage dependence for the internal Ba^{2+} off rate in DRK1 is similar to the interaction of external Ba^{2+} ions with the ATP-sensitive K^+ channels of frog skeletal muscle (15).

Due to the combined effects of depolarization voltage on the on and off rate constants, the K_d showed a marked voltage dependence, with an e-fold decrease for 33 mV and an electrical distance of 0.39 (δ = 0.39).

Effect of Pore Mutations at Position 374 on Blockade by Internal Ba^{2+} Ions

Fig. 7 shows single-channel currents obtained in control and 5 μM internal Ba^{2+} solutions from inside-out oocyte patches

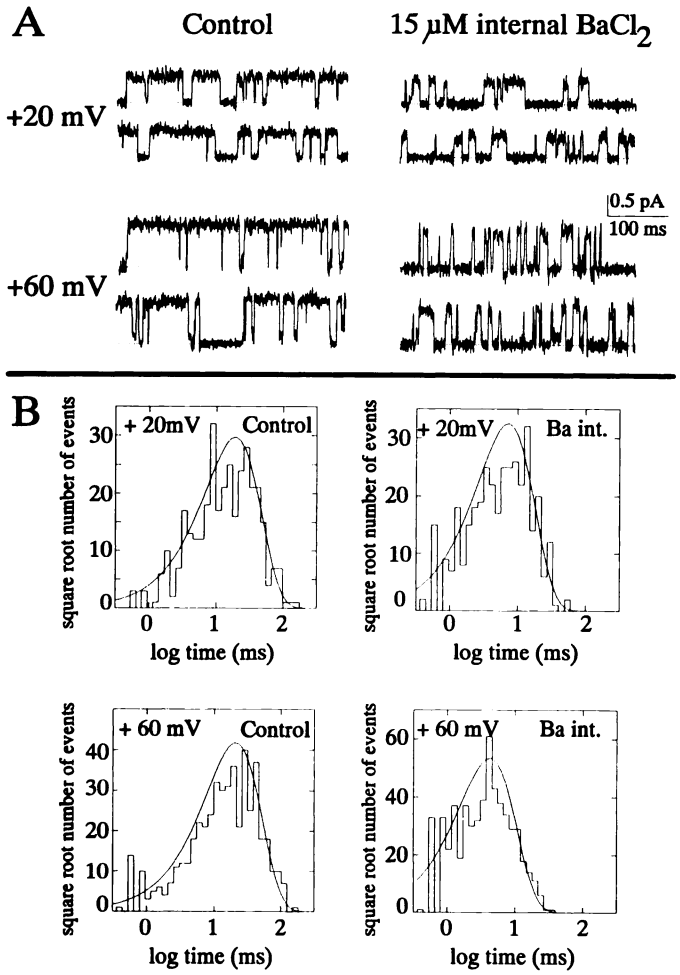

Fig. 4. Voltage dependence of internal Ba^{2+} block of DRK1 channels. A, Representative single-channel *traces* obtained from the same DRK1-containing inside-out patch at +20 mV and +60 mV, both under control conditions and after exposure of the internal side of the patch to 15 μM Ba^{2+} ions. Holding potential, −80 mV; sampling, 5 kHz; filter, 1 kHz. B, Open time histograms for DRK1 channels in the absence and in the presence of 15 μM internal Ba^{2+} at two different voltages (+20 mV and +60 mV). The distributions were obtained from 30–60 traces collected for each of the four experimental conditions (approximately 600–1000 idealized events). The *solid lines* represent the best fits to single-exponential functions having the following time constants: control +20 mV, 20.8 msec; control +60 mV, 22.8 msec; 15 μM Ba^{2+} +20 mV, 7.9 msec; 15 μM Ba^{2+} +60 mV, 4.7 msec.

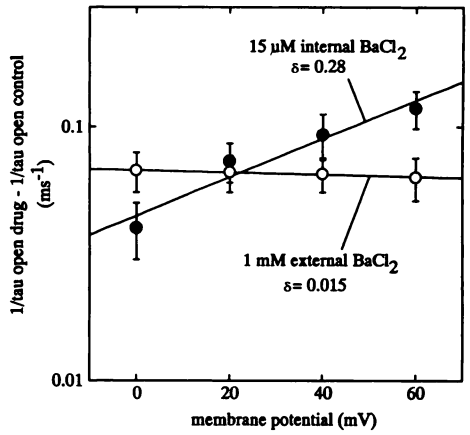

Fig. 5. Voltage dependence of the on rate for external and internal Ba^{2+} ions. The reciprocal of the mean open time of DRK1 channels exposed to either 1 mM external Ba^{2+} ions (○) or 15 μM internal Ba^{2+} ions (●) is plotted as a function of membrane potential. The *solid lines* represent linear regressions fitted to the *experimental points* for both external and internal Ba^{2+} application. From the slope of this regression, the fraction of the membrane field (δ) experienced by the cation in accessing its site can be determined (34, 35). Each *point* is the mean ± standard error of at least four determinations.

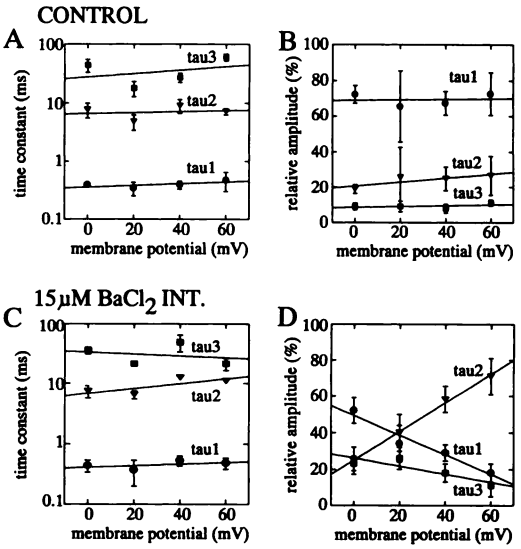

Fig. 6. Voltage dependence of the off rate for internal Ba^{2+} ions. A and C, Voltage dependence of the three closed time exponentials characterizing the closed time histogram in inside-out DRK1 channels under control conditions (A) or with 15 μM Ba^{2+} ions in the internal solution (C). The three exponentials correspond to τ_1, τ_2, and τ_3, as described in the legend to Fig. 3. The *solid lines* represent linear regressions fitted to the *experimental points* for each of the exponentials (τ_1, τ_2, and τ_3). Each *point* is the mean ± standard error of at least four determinations. B and D, Voltage dependence of the relative amplitude of τ_1, τ_2, and τ_3 in inside-out DRK1 channels under control conditions (B) or with 15 μM Ba^{2+} ions in the internal solution (D). The *solid lines* represent linear regressions fitted to the *experimental points* for each of the exponentials (τ_1, τ_2, and τ_3). Each *point* is the mean ± standard error of at least four determinations.

expressing either the wild-type DRK1 channel (Fig. 7A), V374T (Fig. 7B), V374S (Fig. 7C), or V374I (Fig. 7D). In wild-type DRK1 channels, with 5 μM internal Ba^{2+} no modification was observed for the probability of being open, the mean open time, or the mean closed time. In contrast, the same concentration of the divalent cation caused a 70–90% decrease in the probability of being open for both DRK1 V374T and DRK1 V374S channels (Table 1). Analysis of the on and off rate constants for Ba^{2+} with these two channels revealed that, whereas the on rate constant remained practically unmodified, the off rate of the drug was dramatically decreased. For V374T and V374S, internally applied Ba^{2+} ions caused greatly prolonged closed times. In contrast, the substitution of the valine at position 374 with another hydrophobic residue, isoleucine, did not cause any detectable modification of the kinetics of Ba^{2+} block, compared with the wild-type DRK1 channel.

The closed time distributions for V374T channels under control conditions and after application of 5 μM Ba^{2+} ions to the intracellular face of the channel are shown in Fig. 8, A and B, respectively. By analogy to what has already been described for the wild-type channel, in both control and Ba^{2+}-containing solutions the closed interval histograms were accurately described by a sum of three exponentials. The mean values and their mean relative amplitudes are reported in Table 1. It is

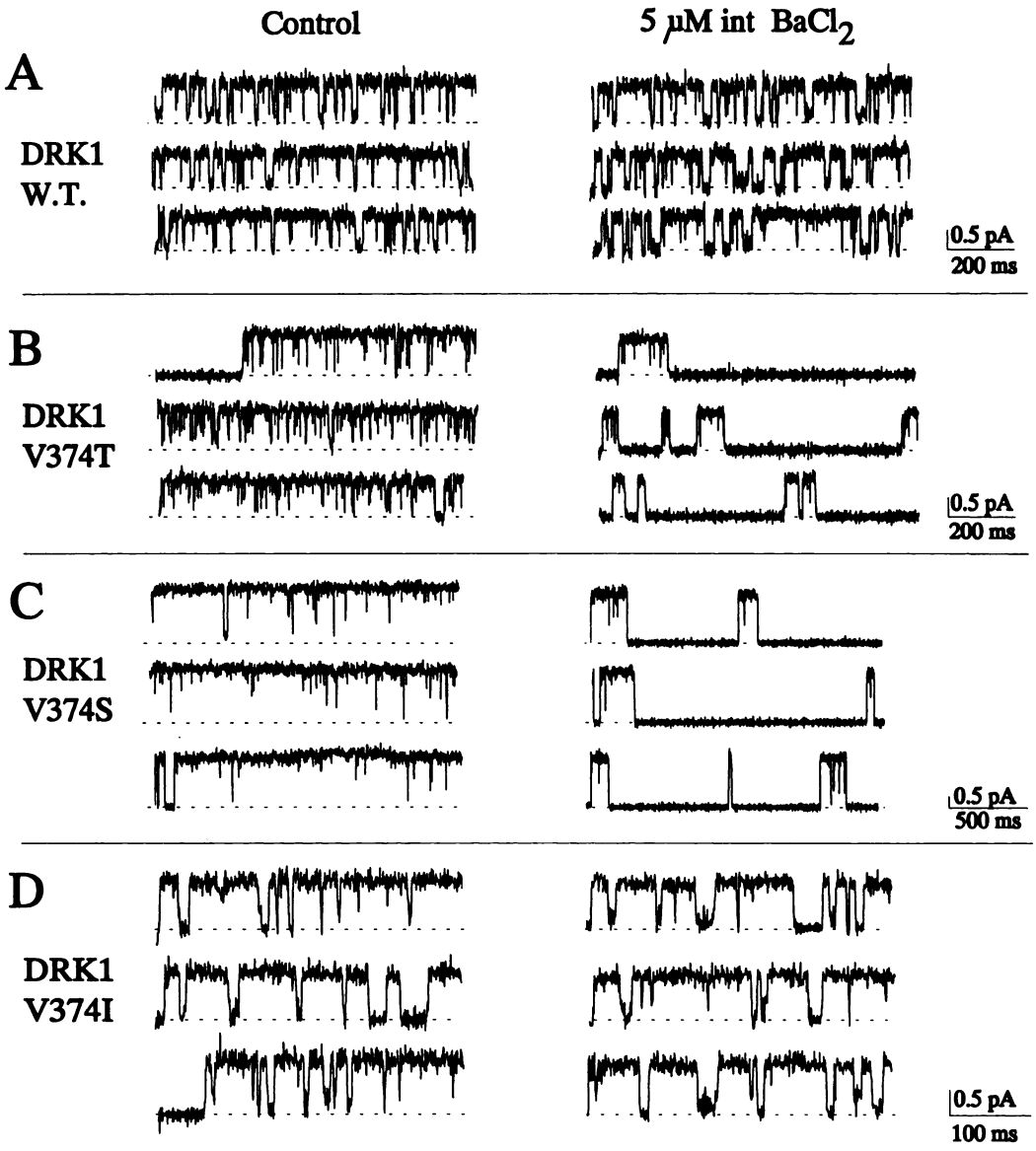

Fig. 7. Effect of internal Ba^{2+} ions on DRK1 channels and DRK1 position 374 mutants V374T, V374S, and V374I. Representative single-channel *traces* obtained from the same inside-out patch containing wild-type (A), DRK1 V374T (B), DRK1 V374S (C), and DRK1 V374I (D), exposed to the control solution (*left*) or to 5 μM Ba^{2+} (*right*). Holding potential, −80 mV; test potential, +40 mV; sampling, 2 kHz for DRK1 and V374T, 1 kHz for V374S, and 5 kHz for V374I; filter, 1 kHz for DRK1 and 500 Hz for V374T, V374S, and V374I. Note the different calibrations for the three different sets of traces, due to the different single-channel amplitudes in the four channels (vertical calibration) and to the longer Ba^{2+}-induced closed states (horizontal calibration). The data in D were obtained with Rb^+ as current carrier, due to the very small K^+ conductance of DRK1 V374I (28).

evident that the relative amplitude of the slowest time constant (τ_3) increased 10-fold (from 0.7% to 7%), suggesting that the Ba^{2+}-induced closed times fell within this time constant (180–250 msec). This value was at least 10 times larger than that seen with the wild-type channel, suggesting that the greater effectiveness of Ba^{2+} ions in blocking the DRK1 V374T and V374S channels was mostly due to a reduced off rate from the channel. In analogy with the wild-type channel, the decrease in the single-channel probability of being open as a function of Ba^{2+} concentration resulted in a K_d of 2 μM at +40 mV.

Due to the very slow time constant introduced by Ba^{2+} ions in DRK1 V374T, truncation errors resulting from the finite length of the depolarizing pulse (from 1 to 2 sec) caused an overestimation of the drug off rate. This suggests that the difference in the K_d between the wild-type and mutated channels may be even greater than the 6–7-fold difference detected in the present experiments.

Due to the very slow off rate of Ba^{2+} ions in DRK1 V374T, the probability of being open decreased with time during the pulse; the ensemble single-channel current of DRK1 V374T channels exposed internally to 5 μM Ba^{2+} therefore showed inactivation (Fig. 8C), which was absent in the wild-type channel exposed to the same (5 μM) or even higher (15 μM) internal Ba^{2+} concentrations (Fig. 8D). This drug-induced inactivation resembled the kinetics of interaction of the divalent cation with the squid giant axon delayed rectifier (10, 12).

Effect of External Ba^{2+} on DRK1 Currents Expressed in *Xenopus* Oocytes

Whole-cell currents. In Fig. 9A are shown the effects of external Ba^{2+} on whole-oocyte K^+ currents. The steady state level of the current was not markedly affected, even at the highest concentration (10 mM) of the divalent cation (<20% block), but there was a marked slowing of the activation kinetics. The decreased rate of activation is shown more clearly in Fig. 9B. This shows the normalized first 125 msec of the current response elicited by a voltage step to +40 mV under control conditions and in the presence of increasing concentrations of external Ba^{2+}. In Fig. 9C, the time constants for macroscopic current activation are plotted as a function of membrane potential. When 10 mM Ba^{2+} was present in the external medium,

TABLE 1
Effects of internal and external Ba^{2+} on DRK1 V374T channels

	Control	5 μM Internal $BaCl_2$	1 mM External $BaCl_2$
Single-channel amplitude at +40 mV (pA)	1.07 ± 0.04	1.1 ± 0.07	1.1 ± 0.2
Mean open time (msec)	15.9 ± 1.2	13.8 ± 1.9	15.9 ± 0.9
Mean closed time (msec)	4.5 ± 0.8	32.9 ± 6.7	5.4 ± 1.2
τ_1 (msec)	0.7 ± 0.1	0.7 ± 0.1	0.7 ± 0.1
τ_2 (msec)	6.4 ± 1.1	10.7 ± 2.7	6.1 ± 0.3
τ_3 (msec)	164 ± 25	218.0 ± 25	135 ± 36
Amplitude of τ_1 (%)	92.3 ± 0.5	82.5 ± 0.3	91.5 ± 0.4
Amplitude of τ_2 (%)	6.9 ± 0.4	8.8 ± 1.5	8.1 ± 0.6
Amplitude of τ_3 (%)	0.7 ± 0.3	7.0 ± 1.0	1.2 ± 0.2
Burst duration (msec)[a]	171.2 ± 22	54.4 ± 15	144 ± 10
No. of openings/burst	10.4 ± 0.6	3.5 ± 0.5	8.7 ± 0.4
Probability of being open (%)[b]	56.8 ± 5.8	13.2 ± 2.2	58.9 ± 4.4
First latency (msec)	87.7 ± 42	133 ± 32	232 ± 42
No. of observations[c]	6	4	3

[a] The burst duration was determined using τ_2 as the critical closed time.
[b] The probability of being open was determined between 300 and 1000 msec after the beginning of the depolarizing pulse.
[c] All the data presented in this table were obtained in inside-out patches (sampling frequency, 1 kHz; filter frequency, 500 Hz).

DRK1 activation kinetics were shifted about 40 mV to the right along the voltage axis. Interestingly, this effect of externally applied Ba^{2+} ions was completely counteracted when the external K^+ concentration was raised from 2.5 mM to 100 mM (Fig. 9C).

If this effect of Ba^{2+} ions were due to an ability to interact with negative charges at the external surface of the membrane, other DRK1 voltage-dependent parameters should show parallel changes in voltage dependence (27). We investigated the effects of the same concentration of Ba^{2+} ions (10 mM) on the steady state activation and inactivation curves for DRK1 (Fig. 9D). External Ba^{2+} ions did not affect the steepness of either of these voltage-dependent parameters. The slope factors of the steady state inactivation curves were 6.7 ± 0.9 and 6.1 ± 0.4 mV/*e*-fold in the absence and in the presence of 10 mM external Ba^{2+}, respectively, whereas the slope factors of the steady state activation curves were 7.6 ± 1.2 and 7.2 ± 0.8 mV/*e*-fold in the absence and in the presence of 10 mM Ba^{2+}, respectively. In contrast, the midpoint potentials for the steady state inactivation curves were −17.6 ± 0.7 and −10.6 ± 1.1 mV in the absence and in the presence of 10 mM external Ba^{2+}, respectively, whereas the midpoint potentials of the steady state activation curves were 10.2 ± 1.7 and 21.1 ± 1.4 in the absence and in the presence of 10 mM Ba^{2+}, respectively (n = 4). Therefore, a positive shift of only 10 mV was induced by Ba^{2+}. These results, together with the observations that 10 mM Ba^{2+} shifted DRK1 deactivation kinetics to the right of the voltage axis by about 10 mV and that a similar concentration (10 mM) of Mg^{2+} ions caused a similar 10-mV shift of all the channel voltage-dependent parameters (steady state activation and inactivation curves and time constant for activation; data not shown), suggest that external Ba^{2+} effects on activation kinetics result from a specific interaction of the divalent ion with an externally accessible site in the channel that modulates activation gating.

Single-channel currents. In Fig. 10A are shown representative single-channel traces recorded from *Xenopus* oocytes using the cell-attached configuration of the patch-clamp technique, both under control conditions (Fig. 10A, *left*) and in the presence of 1 mM Ba^{2+} in the recording pipette (Fig. 10A, *right*). Two prominent effects of Ba^{2+} were observed. The first was a prolongation of the latency to first opening (Fig. 10B); the mean first latency was prolonged from about 30 msec (control) to 80 msec (1 mM Ba^{2+}). Under control condition, the cumulative first latency distribution was described by a double-exponential time course, with a dominant (88.2% relative amplitude) fast component of 21.2 msec and a slower component of 116

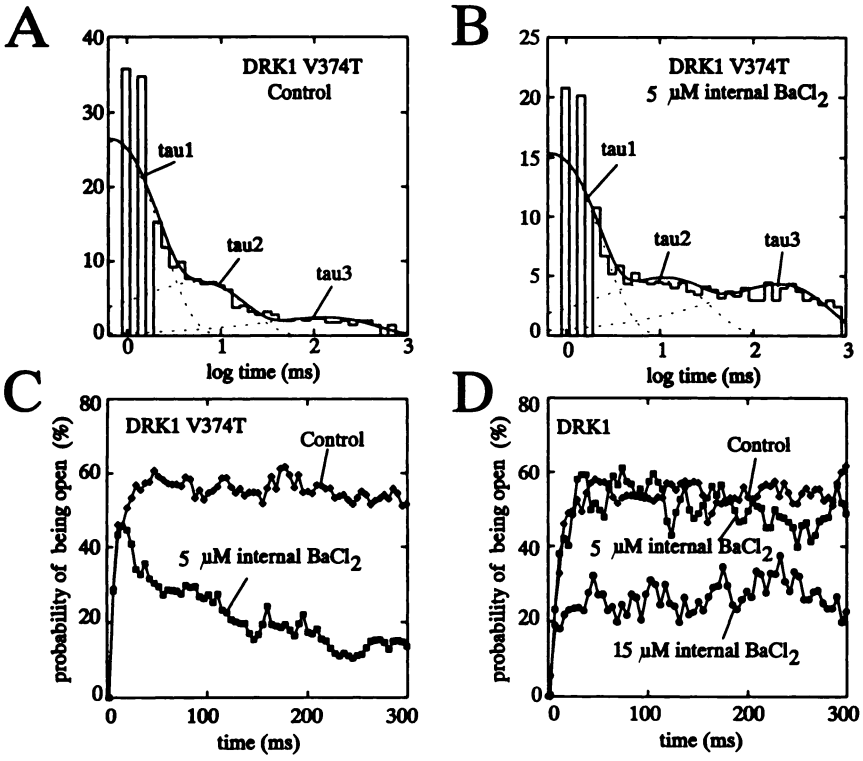

Fig. 8. Closed-time distribution in DRK1 V374T in the absence and in the presence of 5 μM internal Ba^{2+} ions. A and B, Distributions of the DRK1 V374T single-channel closed intervals in inside-out patches under control conditions (A) or after exposure to 5 μM internal Ba^{2+} ions (B). In both cases, three exponentials were required to adequately fit the data. The three peaks were defined as τ_1, τ_2, and τ_3, which correspond to the fastest, the middle, and the slowest time constants of the distribution, respectively, as described in the legend to Fig. 3. Data were pooled from four different inside-out patches exposed to control solution (A) and to 5 μM Ba^{2+} ions (B), to obtain the distributions shown. C, Time course of the open probability of DRK1 V374T channels under control conditions (♦) and upon exposure to 5 μM internal Ba^{2+} (■). The distribution shown is derived from data pooled from three inside-out patches exposed to both conditions (0 and 5 μM internal Ba^{2+}). D, Time course of the open probability of DRK1 channels under control conditions (♦) and upon exposure to 5 μM (■) and 15 μM (●) internal Ba^{2+}. The distribution shown is derived from data pooled from three inside-out patches exposed to the three conditions (0, 5, and 15 μM internal Ba^{2+}).

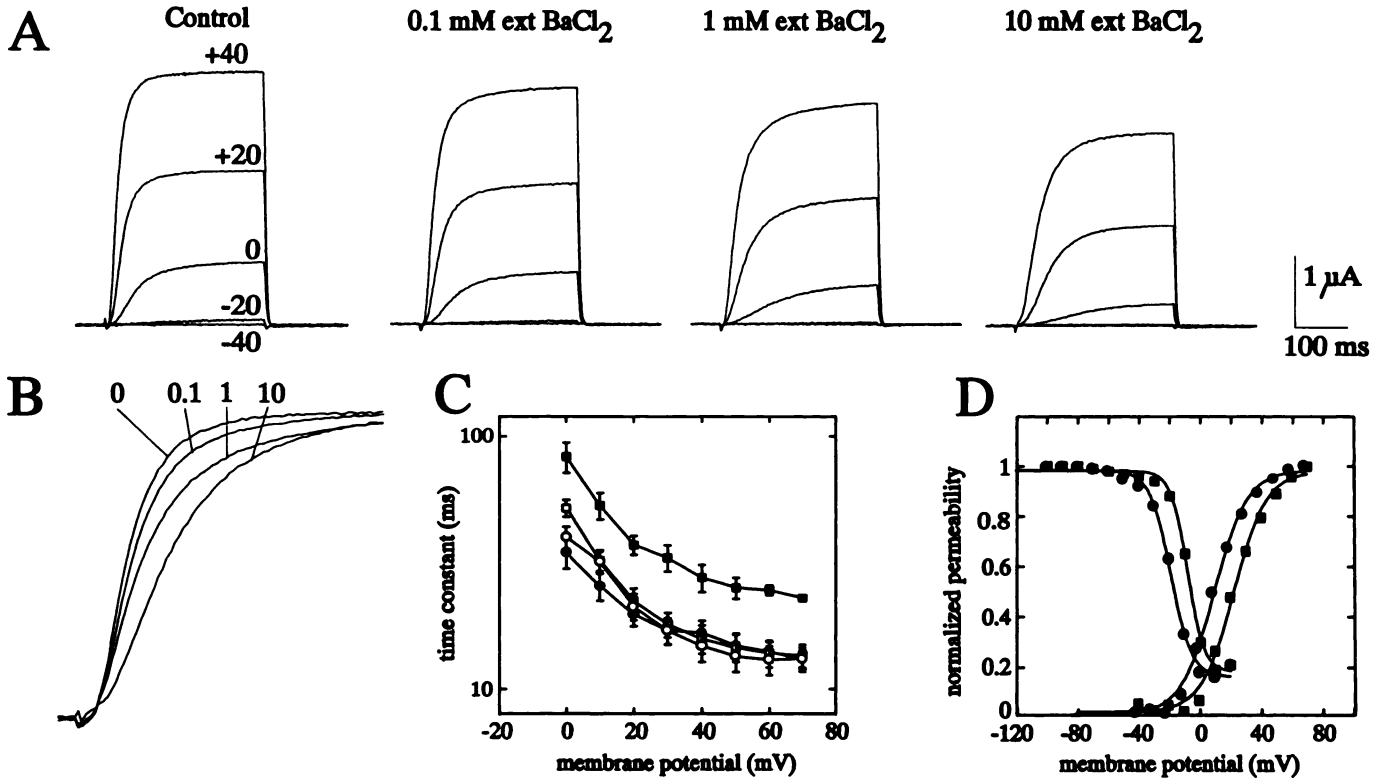

Fig. 9. Effect of external Ba^{2+} on DRK1 whole-cell currents. A, Whole-cell currents from DRK1-injected *Xenopus* oocytes superfused in the presence of the indicated concentrations (0, 0.1, 1, and 10 mM) of external Ba^{2+}. Holding potential, −80 mV; test potentials, −40, −20, 0, +20, and +40 mV. B, Superimposed normalized voltage-clamp current responses to +40 mV depolarizing pulses from DRK1-injected *Xenopus* oocytes superfused in the presence of the indicated concentrations (0, 0.1, 1, and 10 mM) of external Ba^{2+}. Only the first 125 msec are shown. C, Effect of 10 mM external Ba^{2+} on the activation kinetics of DRK1 channels expressed in *Xenopus* oocytes. Activation kinetics were measured as described previously (36). *Closed symbols*, results from experiments performed in a low K^+-containing external solution (120 mM *N*-methyl-D-glucamine, 120 mM MES, 2.5 mM KOH, 2 mM $MgOH_2$, 10 mM HEPES, pH 7.4). ●, Control; ■, 10 mM Ba^{2+}. *Open symbols*, results from experiments performed in high K^+-containing solution (22.5 mM *N*-methyl-D-glucamine, 22.5 mM MES, 100 mM KOH, 2 mM $MgOH_2$, 10 mM HEPES, pH 7.4). ○, Control; □, 10 mM Ba^{2+}. Each value represents the mean ± standard error of four determinations. D, Effect of 10 mM external Ba^{2+} on DRK1 steady state activation and inactivation curves. Steady state activation curves were determined in a low K^+-containing external solution as described previously (36), by converting the current values obtained at the end of a 350-msec voltage-clamp depolarizing pulse to permeability values, using the Goldman-Hodgkin-Katz equation, due to the strong rectification of the instantaneous and single-channel current-voltage relationships. The *solid lines* represent the fits to a Boltzmann distribution of the permeability values at different potentials. Steady state inactivation curves were determined in double-pulse experiments with 10-sec prepulses (36). ●, Control; ■, 10 mM external Ba^{2+}.

msec, which accounted for 11.8% of the total number of observations. When 1 mM Ba^{2+} was present in the pipette, the cumulative first latency distribution still followed double-exponential kinetics, with time constants of 21.8 and 102.8 msec, but the relative amplitude favored the slowest time constant (73.3%), whereas the fastest accounted for only 26.7% of the total number of observations.

In addition to this effect on first latency, the presence of 1 mM external Ba^{2+} decreased mean open time from 15.3 ± 2.1 msec at +40 mV (n = 6 patches) to 7.7 ± 2.5 msec (n = 4 patches). The reciprocal of the open times was unaffected by changes in membrane potential between 0 mV and +60 mV, and the calculated effective valence for the block was <2% (δ = 0.015) (see Fig. 5). Consistent with the weak blockade (<10%) of the whole-cell currents with 1 mM external Ba^{2+}, the probability of being open at the end of a depolarizing pulse only decreased from 43.5 ± 6.6% (n = 6) to 39.2 ± 4.2% (n = 5) at 0 mV. This was a consequence of the fact that the openings were interrupted by very fast (<1 msec) closing events whose mean duration overlapped with the fastest time constant of the closed time distribution observed under control conditions (τ_1; see the third paragraph of Results), as judged from the increase of the relative amplitude of this time constant. The fact that the external Ba^{2+}-induced closed time overlapped with τ_1, which under control conditions accounted for >70% of the closing events, prevented an accurate determination of the voltage dependence of the dissociation rate constant.

In spite of the dramatic increase in internal Ba^{2+} affinity in V374T channels, the affinity for the divalent cation when applied externally did not seem to be modified. In fact, as shown in Table 1, when 1 mM Ba^{2+} was present in the pipette the probability of being open was not affected for either wild-type or mutant channels. A 2.5-fold reduction in channel activation kinetics, as reflected in the latency to the first opening, was also observed in V374T channels with external Ba^{2+} and is quantitatively similar to that seen for DRK1 wild-type channels. This suggests that the external site at which Ba^{2+} acts to prolong activation kinetics remained unmodified, despite the dramatic effects of the V374T mutation on the internal Ba^{2+} blocking kinetics. The fact that the V374T mutation does not affect the binding of externally accessible blocking molecules seems also to be supported by the fact that with this mutant, whereas internal TEA affinity was dramatically decreased (28), the affinity for blockade by external TEA was unmodified (the

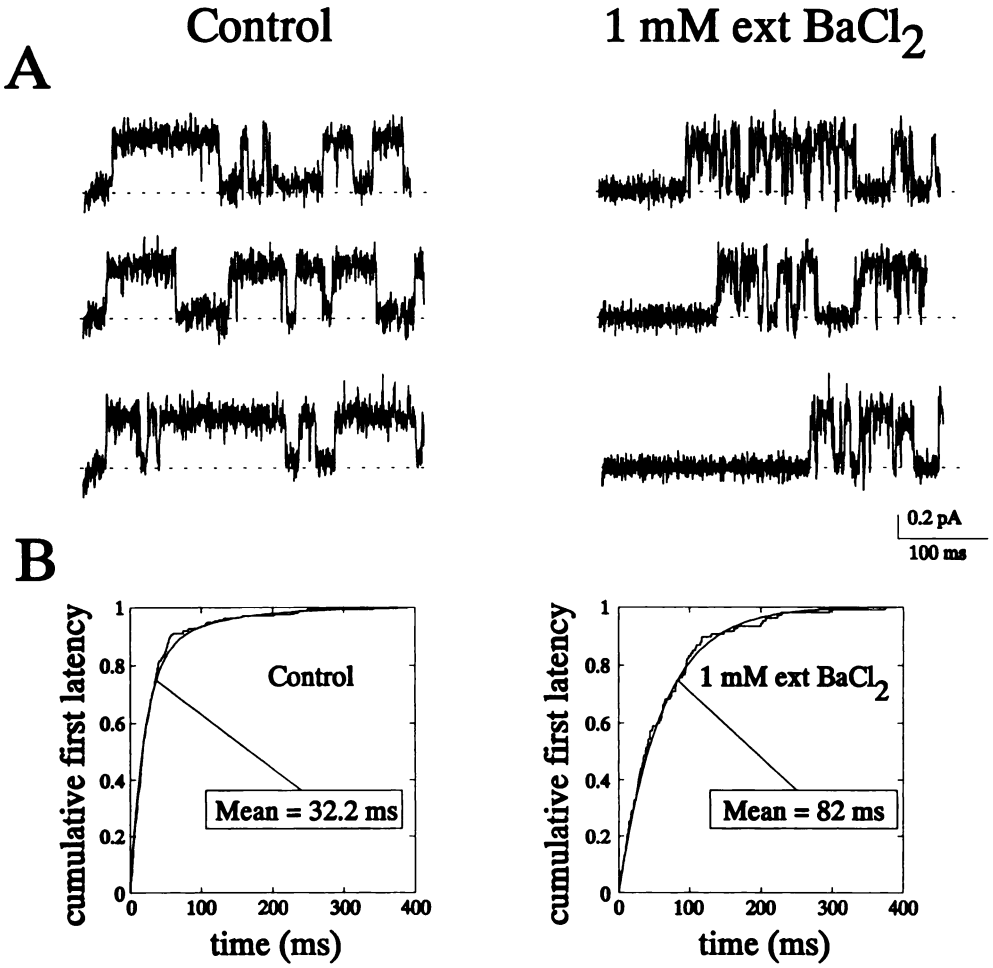

Fig. 10. Effect of external Ba^{2+} on DRK1 single-channel currents. A, Representative single-channel *traces* from two cell-attached patches containing DRK1 channels expressed in *Xenopus* oocytes, in the absence (*left*) and presence (*right*) of 1 mM external Ba^{2+}. Holding potential, −80 mV; test potential, 0 mV; sampling, 5 kHz; filter, 1 kHz. The two patches were obtained in the same oocyte. B, Cumulative first latencies of DRK1 channels in cell-attached patches under control conditions (*left*) and in the presence of 1 mM external Ba^{2+} (*right*). Holding potential, −80 mV; test potential, 0 mV. *Left*, data were obtained from 332 records pooled from six control cell-attached patches; *right*, data were obtained from 236 records pooled from four cell-attached patches in which 1 mM Ba^{2+} was added to the pipette solution.

K_d at +40 mV was 5.5 ± 1.3 mM, n = 5, for the wild-type channel and 5.2 ± 1.5 mM, n = 5, for the V374T mutant channel).

In addition, the mean open time of DRK1 V374T channels was not reduced by external application of Ba^{2+} (Table 1), as was observed with the wild-type channel. This can be ascribed to the lower recording bandwidth of these experiments (sampling rate, 1–2 kHz versus 5 kHz; filter, 500 Hz versus 1 kHz) and to the fact that for V374T the fast closing events (<1 msec), which are sensitive to the reduced bandwidth, accounted for >90% of the closures under control conditions.

In conclusion, it appears that the V374T mutation has not affected the external site for Ba^{2+} block.

Discussion

External and internal blockade by Ba^{2+}. Using a combination of whole-cell and single-channel current measurements in *Xenopus* oocytes expressing the cloned delayed rectifier DRK1, we have shown that Ba^{2+} ion exerts different effects, depending primarily on the side of application. When present on the external side of the channel, the dominant effect is a decreased rate of activation that, at the single-channel level, is reflected in a doubling of the latency to the first opening. This effect appears to arise from interaction between external Ba^{2+} and a specific site in the channel, rather than from a surface charge effect, because the shift in the voltage dependence of the rate of activation is about 4 times greater than the shifts in steady state activation and inactivation. We suggest that external Ba^{2+} ion interacts with the closed state of the channel. Interestingly, this effect of external Ba^{2+} on activation kinetics can be inhibited by increasing the external K^+ concentration to 100 mM. In addition to the slowing of activation gating, external Ba^{2+} caused a fast block of the open channel. At a membrane potential of 0 mV, the on and off rates for the drug were about 0.13 $msec^{-1}$ mM^{-1} and 3 $msec^{-1}$, respectively, resulting in a K_d of 23 mM. The fast off rate explains the small effects on the probability of being open achieved at the concentrations of 1 and 10 mM. However, it should be noted that, in the Ca^{2+}-activated K^+ channels from skeletal muscle (11), the much lower affinity of the external versus internal Ba^{2+} block has been interpreted as a consequence of the 3000 times slower on rate, whereas the off rate for the blocker appears to be identical, irrespective of the side of application. The site at which external Ba^{2+} ions act to determine this fast open-channel block does not appear to be located within the membrane electric field, because the on rate for the drug did not show any potential dependence. It is possible that both effects were produced from a single site, but we cannot exclude separate sites for each effect.

In contrast, application of internal Ba^{2+} resulted in a more potent (K_d, 13 μM) voltage-dependent blockade of wild-type single-channel currents. Based on a Hill coefficient greater than 1 and a nonlinear effect of Ba^{2+} concentrations on association rates, we propose that internal Ba^{2+} ions block DRK1

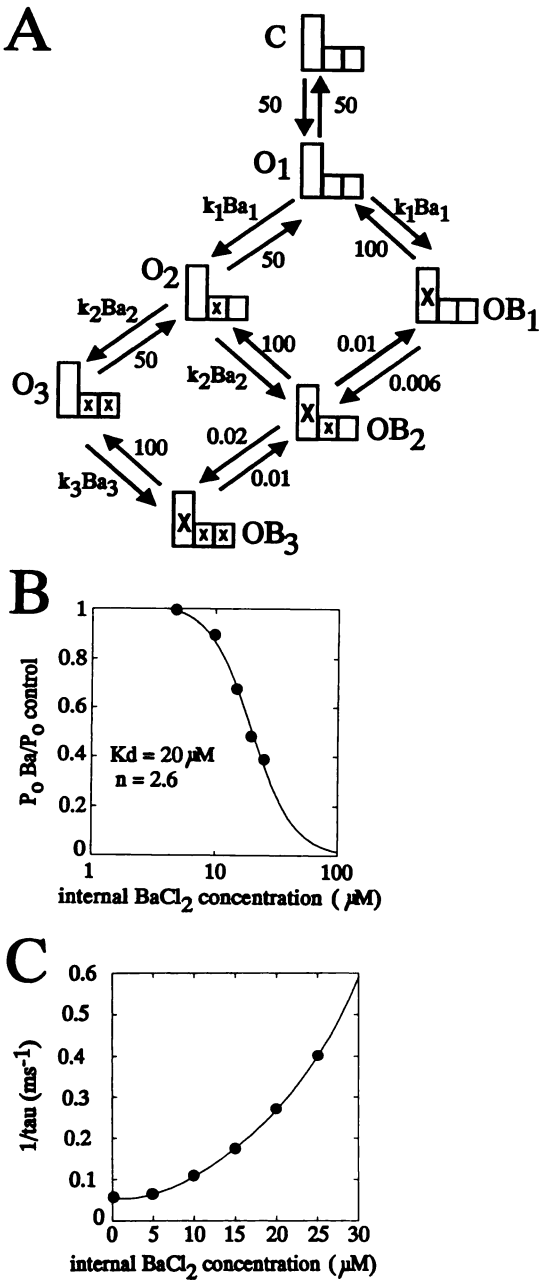

Fig. 11. Multisite binding and blockade by internal Ba^{2+}. A, Markov model of binding. Transition from O_1 to OB_1 is due to blockade of the pore by Ba^{2+}. Transitions from O_1 to O_2 and from O_2 to O_3 result from Ba^{2+} binding to sites near the inner mouth of the pore. Transitions from O_2 to OB_2 and from O_3 to OB_3 are due to blockade of the pore by Ba^{2+}. Cooperativity was introduced by having the forward rate constants for Ba^{2+} association coupled to each other; k_{1Ba1} is 1.5×10^6 M^{-1} sec^{-1}, k_{2Ba2} is 3×10^6 M^{-1} sec^{-1}, and k_{3Ba3} is 10^7 M^{-1} sec^{-1}. These rates simulate the data obtained with 5 μM internal Ba^{2+} ions. The data at higher Ba^{2+} concentrations were simulated by increasing proportionally and simultaneously all three rates (k_{1Ba1}, k_{2Ba2}, and k_{3Ba3}). B, Simulated dose-response curve for blockade by internal Ba^{2+}. K_d is 20 μM and the Hill coefficient (n) equals 2.6. The data closely resemble the experimental results shown in Fig. 2A. C, Blocking rate as a function of internal Ba^{2+} concentration. The simulated data closely resemble the experimental results shown in Fig. 2B.

channels by binding to several sites that show positive cooperativity. This cooperativity for Ba^{2+} block has not been described previously, because in both the Ca^{2+}-activated (11, 13, 14) and the squid axon delayed rectifier (10, 12) K^+ channels internal Ba^{2+} block displayed all the kinetic properties of simple bimolecular reactions, even though the same experiments clearly documented simultaneous occupancy of the pore by blocking and permeating cations.

To explain our results, we have developed the model shown in Fig. 11. In this model, the closed states were lumped together in one state. Cooperativity was achieved by hypothesizing the existence of two binding sites for Ba^{2+} outside the inner mouth of the pore (O_2 and O_3 in Fig. 11A), which would change the rate at which Ba^{2+} blocks the pore at a site about 30% of the way across the membrane field from its inner mouth (OB_1, OB_2, and OB_3). As suggested by the data presented, the association step was allowed to be concentration dependent, whereas the exit rates from the blocked states (OB_1, OB_2, and OB_3) were identical and concentration independent. The equilibrium block produces dose-response curves that simulate the experimental data very closely at lower concentrations. However, at higher concentrations the simulations are not as satisfactory (Fig. 11B). Also at higher concentrations the curve relating blocking rate to Ba^{2+} concentration is too flat (Fig. 11C). Both fits could probably be improved by adding additional sites outside the inner pore mouth and by allowing slight differences in the exit rates from the three blocked sites. It should be noted that our model predicts that the frequency distribution of open times should have three time constants. We attribute our failure to identify the additional time constants and the deviations in the blocking rate-concentration curve and the dose-response curve to effects of noise and limited bandwidth on rapid closures and openings.

Identification of internal Ba^{2+} blocking site by mutational analysis. If K^+ ions interact with sites in the DRK1 channel protein in their dehydrated state (29), it appears likely that, due to the close similarity in the crystal diameters of K^+ (0.266 nm) and Ba^{2+} (0.270 nm), Ba^{2+} ions may bind to structures normally used for K^+ binding to establish high selectivity for this monovalent cation, as suggested in Ca^{2+}-activated K^+ channels (11). This consideration, together with the multi-ion properties of DRK1 revealed by the present experiments (30–31), prompted us to identify channel mutations that were able to affect block by internal Ba^{2+} ions. Position 374 clearly seems to play a crucial role; in fact, when the valine residue in the wild-type channel was substituted with threonine or serine, the dissociation speed of the drug from its internal site(s) of action was decreased >10-fold. The differences in free energy of binding were about 1 kcal/mol, and one possibility that could account for this difference might be enhanced hydrogen bonding of a water molecule associated with Ba^{2+} to the newly introduced hydroxyl group at position 374. In contrast, no change was detected when the valine was substituted by the nonpolar amino acid isoleucine.

In both DRK1 and DRK/NGK (6), a chimeric channel produced from DRK1 (16) and NGK2 (32), the nature of the residues at position 374 clearly regulated the channel conductance for K^+ (4), as well as that for Rb^+ ions (7, 28). This view seems to be supported by the recent cloning of two K^+ channel genes from T lymphocytes, which, in the S_5-S_6 linker region, differ only at a residue corresponding to position 374 (33).

Channels encoded by these genes have different K^+ versus Rb^+ selectivity and sensitivity to internal TEA blockade. It appears likely that, in DRK1, position 374 represents an important binding site where cation discrimination and ion selectivity occur. The present results indicate that this position is at the surface at the inner end of K^+ pores.

To summarize, using mutational analysis we have identified two sites, one at each end of K^+ pores, with which Ba^{2+} interacts. The presence of such sites was suggested earlier (10–15). Moreover, in the present K^+ channel additional binding sites, possibly located near the pore, appear to be present.

Acknowledgments

The authors wish to thank G. Schuster and Wei-Qiang Dong for oocyte injection and handling and Mary Champagne for molecular biology technical support.

References

1. MacKinnon, R., and C. Miller. Mutant potassium channels with altered binding of charybdotoxin, a pore-blocking peptide inhibitor. *Science (Washington D. C.)* **245**:1382–1385 (1989).
2. MacKinnon, R., and G. Yellen. Mutations affecting TEA blockade and ion permeation in voltage-activated K^+ channels. *Science (Washington D. C.)* **250**:276–279 (1990).
3. Yellen, G., M. Jurman, T. Abramson, and R. MacKinnon. Mutations affecting internal TEA blockade identify the probable pore-forming region of a K^+ channel. *Science (Washington D. C.)* **251**:939–942 (1991).
4. Kirsch, G. E., J. A. Drewe, H. A. Hartmann, M. Taglialatela, M. De Biasi, A. M. Brown, and R. H. Joho. Differences between the deep pores of K^+ channels determined by an interacting pair of non-polar amino acids. *Neuron* **8**:499–505 (1992).
5. Yool, A. J., and T. L. Schwarz. Alteration of ionic selectivity of a K^+ channel by mutation of the H5 region. *Nature (Lond.)* **349**:700–704 (1991).
6. Hartmann, H. A., G. E. Kirsch, J. A. Drewe, M. Taglialatela, R. H. Joho, and A. M. Brown. Exchange of conduction pathways between two related K^+ channels. *Science (Washington D. C.)* **251**:942–944 (1991).
7. Kirsch, G. E., J. A. Drewe, M. Taglialatela, H. A. Hartmann, and A. M. Brown. A single non-polar residue in the deep pore of related K^+ channels acts as a K^+:Rb^+ conductance switch. *Biophys. J.* **62**:136–144 (1992).
8. Guy, H. R., and F. Conti. Pursuing the structure and function of voltage-gated channels. *Trends Neurosci.* **13**:201–206 (1990).
9. Durrell, R., and H. R. Guy. Atomic scale structure and functional models of voltage-gated potassium channels. *Biophys. J.* **62**:238–250 (1992).
10. Armstrong, C. M., R. P. Swenson, and S. R. Taylor. Block of squid axon K channels by internally and externally applied barium ions. *J. Gen. Physiol.* **80**:663–682 (1982).
11. Miller, C., R. Latorre, and I. Reisin. Coupling of voltage-dependent gating and Ba^{++} block in the high-conductance, Ca^{++}-activated K^+ channel. *J. Gen. Physiol.* **90**:427–449 (1987).
12. Eaton, D. C., and M. S. Brodwick. Effect of barium on the potassium conductance of squid axon. *J. Gen. Physiol.* **75**:727–750 (1980).
13. Vergara, C., and R. Latorre. Kinetics of Ca^{2+}-activated K^+ channels from rabbit muscle incorporated into planar bilayers: evidence for a Ca^{2+} and Ba^{2+} blockade. *J. Gen. Physiol.* **82**:543–568 (1983).
14. Neyton, J., and C. Miller. Discrete Ba^{2+} block as a probe of ion occupancy and pore structure in the high-conductance Ca^{2+}-activated K^+ channel. *J. Gen. Physiol.* **92**:569–586 (1988).
15. Quayle, J. M., N. B. Standen, and P. R. Stanfield. The voltage-dependent block of ATP-sensitive potassium channels of frog skeletal muscle by caesium and barium ions. *J. Physiol. (Lond.)* **405**:677–697 (1988).
16. Frech, G. C., A. M. J. VanDongen, G. Schuster, A. M. Brown, and R. H. Joho. A novel potassium channel with delayed rectifier properties isolated from rat brain by expression cloning. *Nature (Lond.)* **340**:642–645 (1989).
17. Moorman, J. R., G. E. Kirsch, A. M. Brown, and R. H. Joho. Changes in sodium channel gating produced by point mutations in a cytoplasmic linker. *Science (Washington D. C.)* **250**:688–691 (1990).
18. Maniatis, T., E. F. Fritsch, and J. Sambrook. *Molecular Cloning. A Laboratory Manual.* Cold Spring Harbor Laboratory, Cold Spring Harbor, NY (1982).
19. Joho, R. H., J. R. Moorman, A. M. J. VanDongen, G. E. Kirsch, H. Silberberg, G. Schuster, and A. M. Brown. Toxin and kinetic profile of rat brain type III sodium channels expressed in *Xenopus* oocytes. *Mol. Brain Res.* **7**:105–113 (1990).
20. Fabiato, A., and F. Fabiato. Calculator programs for computing the composition of the solutions containing multiple metals and ligands used for experiments in skinned muscle cells. *J. Physiol. (Paris)* **75**:463–505 (1979).
21. VanDongen, A. M. J. Transit: a new algorithm for analyzing single ion channel data containing multiple conductance levels. *Biophys. Soc. Annu. Meet. Abstr.* **61**:A256 (1992).
22. Linbird, L. *Cell Surface Receptors: A Short Course on Theory and Methods.* Martinus Nijhoff Publishing, Norwell, MA (1986).
23. Taglialatela, M., A. M. J. VanDongen, J. A. Drewe, R. H. Joho, A. M. Brown, and G. E. Kirsch. Patterns of internal and external tetraethylammonium block in four homologous K^+ channels. *Mol. Pharmacol.* **40**:299–307 (1991).
24. Heginbotham, L., and R. MacKinnon. The aromatic binding site for tetraethylammonium ion on potassium channels. *Neuron* **8**:483–491 (1992).
25. Christie, M. J., R. A. North, P. B. Osborne, J. Douglass, and J. P. Adelman. Heteropolymeric potassium channels expressed in *Xenopus* oocytes from cloned subunits. *Neuron* **4**:405–411 (1990).
26. Davies, N. W., A. E. Spruce, N. B. Standen, and P. R. Stanfield. Multiple blocking mechanisms of ATP-sensitive potassium channels of frog skeletal muscle by tetraethylammonium ions. *J. Physiol. (Lond.)* **413**:31–48 (1989).
27. Lester, H. A. Strategies for studying permeation at voltage-gated ion channels. *Annu. Rev. Physiol.* **53**:477–496 (1991).
28. Taglialatela, M., J. A. Drewe, H. A. Hartmann, G. E. Kirsch, and A. M. Brown. Regulation of K^+/Rb^+ selectivity and internal TEA blockade by mutations at a single site in K^+ pores. *Pflügers Arch.* **423**:104–112 (1993).
29. Hille, B. Selective permeability: saturation and binding, in *Ionic Channels of Excitable Membranes.* Sinauer Associates Inc., Sunderland, 362–389 (1992).
30. Hille, B., and W. Schwarz. Potassium channels as multi-ion single-file pores. *J. Gen. Physiol.* **72**:409–442 (1978).
31. Yellen, G. Permeation in potassium channel: implications for channel structure. *Annu. Rev. Biophys. Chem.* **16**:227–246 (1987).
32. Yokoyama, S., K. Imoto, T. Kawamura, H. Higashida, N. Iwabe, T. Miyata, and S. Numa. Potassium channels from NG108–15 neuroblastoma-glioma hybrid cells. *FEBS Lett.* **259**:37–42 (1989).
33. Grissmer, S., J. Aivar, R. Wymore, A. Nguyen, R. Spencer, and K. G. Chandy. Does a single residue in the pore determine sensitivity to TEA, single channel conductance and ion selectivity in T-cell K^+ channels? *Soc. Neurosci. Abstr.* **18**:920 (1992).
34. Woodhull, A. M. Ionic blockage of sodium channels in nerve. *J. Gen. Physiol.* **61**:687–708 (1973).
35. Kirsch, G. E., M. Taglialatela, and A. M. Brown. Internal and external TEA block in single cloned K^+ channels. *Am. J. Physiol.* **30**:C583-C590 (1991).
36. VanDongen, A. M. J., G. C. Frech, J. A. Drewe, R. H. Joho, and A. M. Brown. Alteration and restoration of K^+ channel function by deletions at the N- and C-termini. *Neuron* **5**:433–443 (1990).

Send reprint requests to: Maurizio Taglialatela, Department of Molecular Physiology and Biophysics, Baylor College of Medicine, One Baylor Plaza, Houston, TX 77030.